Nuclear Engineering and Design 429 (2024) 113602

Contents lists available at ScienceDirect

Nuclear Engineering and Design

journal homepage: www.elsevier.com/locate/nucengdes

Two-phase modelling for fission gas sweeping in restructuring nuclear oxide fuel

G. Zullo [a], A. Scolaro [b], T. Barani [c], D. Pizzocri [a,*]

[a] Politecnico di Milano, Department of Energy, Nuclear Engineering Division, Via La Masa 34, 20156, Milano, Italy
[b] École Polytechnique Fédérale de Lausanne (EPFL), Laboratory for Reactor Physics and System Behaviour, 1015 Lausanne, Switzerland
[c] Commissariat á l'Énergie Atomique et aux Énergies Alternatives, DES/IRESNE/DEC/SESC, Saint-Paul-lez-Durance Cedex, 13108, France

ARTICLE INFO

Keywords:
Uranium dioxide
High burnup structure
SCIANTIX
Two-phase flow

ABSTRACT

In this work, we propose a modelling approach for the intra-granular fission gas behaviour in UO_2 under restructuring process. Leveraging the definition of restructured volume fraction, we consider the fuel matrix transition from the non-restructured to the restructured phase, together with the evolution of the corresponding fission gas concentrations retained in the fuel matrix. Firstly, we derive a sweeping term that exchanges fission gas atoms from the non-restructured to the restructured fuel region. The sweeping term is then included in the conventional intra-granular fission gas diffusion problem. Secondly, the spectral diffusion algorithm is employed to solve two spatially-dimensionless problems, properly representing the non-restructured region with micrometric grains and the restructured region with sub-micrometric grains. The model developed is implemented in SCIANTIX, a 0D meso-scale code for physics-based modelling of fission gas behaviour in nuclear oxide fuel and compared with experimental data and semi-empirical models.

1. Introduction

It is known that in the rim region of UO_2 nuclear fuel pellets, the combination of high local burnup and low temperature induces a UO_2 phase transition, or restructuring process, with the formation of the HBS (Walker et al., 1992; Cunningham et al., 1992; Khvostov et al., 2005; Veshchunov and Shestak, 2009; Pizzocri et al., 2017; Wiss et al., 2017; Rest et al., 2019; Barani et al., 2020, 2022; Cappia et al., 2022). Typical thresholds for initiating the HBS identify local burnups higher than 45-50 GWd/tU (connected to high radiation damage and fission product concentration) and temperatures lower than the recovery threshold temperature of 1273.15 K (Wiss et al., 2017; Cappia et al., 2022; Spino et al., 2006; Cappia et al., 2016; Gerczak et al., 2018; McKinney et al., 2023). As reported in previous experimental (Wiss et al., 2017; Cappia et al., 2022; McKinney et al., 2023; Spino et al., 2005; Noirot et al., 2008) modelling (Khvostov et al., 2005; Veshchunov and Shestak, 2009; Pizzocri et al., 2017; Barani et al., 2020, 2022), the HBS formation involves an accumulation of dislocation defects, the polygonization/recrystallisation of micrometric grains into sub-micrometric grains[1] without extended defects (Cappia et al., 2022; Spino et al., 2006; McKinney et al., 2023), the decrease of the intra-granular fission gas concentration (also known as depletion), and the formation of a novel population of inter-granular spherical pores that accumulate fission gas. Properly modelling the formation and evolution of the HBS is critical for fuel rod fuel performance since it impacts the material properties (e.g., thermal conductivity, elastic modulus). This represents a potential concern for the safe operation of nuclear fuel to extended burnups. For instance, slow temperature changes at burnup values above 60 MWd/kgU can trigger fine fuel fragmentation phenomenon, posing safety issues during design-basis accidents, such as reactivity-initiated accidents and loss-of-coolant accidents (Jernkvist, 2019, 2020).

In particular, in this brief work, we deal with the modelling of the fission gas depletion problem, this being the fundamental starting point to provide a solid representation of (i) the distribution of fission gas that accumulates inside inter-granular cavities and HBS porosity, and (ii) the smooth phase transition from the non-restructured UO_2 matrix to the restructured one. Both semi-empirical (Lassmann et al., 1995a; Lemes et al., 2014; Pizzocri et al., 2017) and mechanistic models (Barani et al.,

* Corresponding author.
E-mail address: davide.pizzocri@polimi.it (D. Pizzocri).

[1] It is worth recalling that the detailed High Burnup Structure (HBS) formation mechanisms are still debated. As explained in Barani et al. (2020), recrystallisation implies the formation and growth of sub-grains (Burke and Turnbull, 1952). Polygonization is the subdivision of original grains into sub-grains. Recent experimental analyses support the polygonization theory, with the increasing concentration of high-angle grain boundaries in the HBS region (Gerczak et al., 2018; McKinney et al., 2023).

https://doi.org/10.1016/j.nucengdes.2024.113602
Received 12 June 2024; Received in revised form 24 July 2024; Accepted 16 September 2024
Available online 28 September 2024

2020) are available in the literature, representing the fission gas depletion of HBS in UO_2. The most mechanistic approach was provided in the work of Barani et al. (2020), in which the authors started from a proper re-fitting of the restructured volume fraction and then solved two intra-granular problems, one for each phase, considering two different integration domains, characterised by their grain size (e.g., micrometric in the as-fabricated region and sub-micrometric in the restructured region). The two intra-granular problems were solved concomitantly with an HBS sweeping condition, given by the conservation of the total concentration of gas in the considered control volume.

This brief work aims to develop a more natural description of the intra-granular gas evolution in uranium dioxide during the restructuring process. Firstly, we derive a sweeping term that exchanges mass from the non-restructured UO_2 to the restructured UO_2. The sweeping term can be included in the intra-granular gas diffusion problem, avoiding further constraints. Secondly, by leveraging the spectral diffusion algorithm for the intra-granular fission gas problem, we avoid dealing with two different integration domains (micrometric and sub-micrometric grains) and solve a single spatial dimensionless problem (i.e., considering the same eigenfunctions). The model developed is implemented in SCIANTIX, a 0D meso-scale code for physics-based modelling of fission gases in nuclear oxide fuel (Zullo et al., 2023; Pizzocri et al., 2020), and compared with experimental data (Walker, 1999) and semi-empirical models (Lassmann et al., 1995a).

The work is structured as follows: Section 2 illustrates the model derivation, Section 3 presents the model application to the fission gas depletion process, Section 4 deals with the results and corresponding discussion, and Section 5 draws the conclusion and points out future applications of the model.

2. Model derivation

The model derivation stems from using the restructured volume fraction α (/) to model the HBS formation rate in uranium dioxide. Hence, we consider a unidirectional phase change from a non-restructured phase (N) to a restructured one (R), with the evolution of two fission gas concentrations, C_N and C_R.

2.1. Phase evolution without exchange term

Given a control volume V, we label $V_R = \alpha V$ as the restructured (i.e., developed HBS) volume region, and $V_N = (1-\alpha)V$ as the non-restructured one (as-fabricated microstructure). Then, C_T is the total concentration of fission gas atoms (i.e., gas in restructured and non-restructured regions) over the total volume V. Similarly, C_N is the concentration of gas atoms in the non-restructured volume V_N, and C_R is the concentration of gas atoms in the restructured volume V_R. The link among these quantities is expressed by:

$$C_T = \alpha C_R + (1-\alpha) C_N \tag{1}$$

Afterwards, we define the following concentrations:

- $C_1 = (1-\alpha)C_N$, representing the concentration of gas in the non-restructured region, referred to the total volume V.
- $C_2 = \alpha C_R$, representing the concentration of gas in the restructured region, referred to the total volume V.

We compute the balance of gas atoms N and R in their respective volumes V_N and V_R, invoking the mass conservation principle:

$$\frac{\partial}{\partial t}\int C_N \, dV_N = \int D_N \nabla^2 C_N \, dV_N + \int S \, dV_N \tag{2}$$

$$\frac{\partial}{\partial t}\int C_R \, dV_R = \int D_R \nabla^2 C_R \, dV_R + \int S \, dV_R \tag{3}$$

In Eqs. (2) and (3), we assume a uniform production rate S of gas atoms per unit volume. Also, we assume that in the restructured region V_R, the diffusivity D_R differs from the one characterising the non-restructured region D_N. It must be noted that Eqs. (2) and (3) are valid in the (initial) assumption of no mass exchanges between the two regions. In particular, from the non-restructured region N to the restructured region R. This assumption will be removed later in the text after deriving a suitable exchange term (Section 2.2).

After introducing the restructured volume fraction α, we can refer the previous balance over the total volume V by substituting $dV_N = (1-\alpha)\, dV$ and $dV_R = \alpha \, dV$:

$$\frac{\partial}{\partial t}\int C_N \, (1-\alpha) \, dV = \int D_N \nabla^2 C_N \, (1-\alpha) \, dV + \int S(1-\alpha) \, dV \tag{4}$$

$$\frac{\partial}{\partial t}\int C_R \, \alpha \, dV = \int D_R \nabla^2 C_R \, \alpha \, dV + \int S\alpha \, dV \tag{5}$$

The arbitrariness of V allows us to convert the integral equations into the local relations, obtaining the following rate equations that are referred to the total control volume V:

$$\frac{\partial}{\partial t}((1-\alpha)C_N) = D_N \nabla^2((1-\alpha)C_N) + (1-\alpha)S \tag{6}$$

$$\frac{\partial}{\partial t}(\alpha C_R) = D_R \nabla^2(\alpha C_R) + \alpha S \tag{7}$$

or equivalently:

$$\frac{\partial C_1}{\partial t} = D_N \nabla^2 C_1 + (1-\alpha)S \tag{8}$$

$$\frac{\partial C_2}{\partial t} = D_R \nabla^2 C_2 + \alpha S \tag{9}$$

Eqs. (8) and (9) represent the evolution of the concentrations C_1 and C_2 over the total volume V. As anticipated, these two equations lack an exchange term that should influence both.

Additionally, it is possible to work out Eqs. (6) and (7) by considering that restructured volume fraction α varies with time, to obtain the following differential equations for C_N and C_R. First, we develop the product derivatives:

$$\frac{\partial}{\partial t}((1-\alpha)C_N) = -\frac{\partial \alpha}{\partial t} C_N + (1-\alpha)\frac{\partial C_N}{\partial t} \tag{10}$$

$$\frac{\partial}{\partial t}(\alpha C_R) = \frac{\partial \alpha}{\partial t} C_R + \alpha \frac{\partial C_R}{\partial t} \tag{11}$$

Then, we combine Eqs. (6), (7) with Eqs. (10), (11), to get:

$$\frac{\partial C_N}{\partial t} = D_N \nabla^2 C_N + S + \frac{1}{1-\alpha}\frac{\partial \alpha}{\partial t} C_N \tag{12}$$

$$\frac{\partial C_R}{\partial t} = D_R \nabla^2 C_R + S - \frac{1}{\alpha}\frac{\partial \alpha}{\partial t} C_R \tag{13}$$

where the last terms represent:

- $+\frac{1}{1-\alpha}\frac{\partial \alpha}{\partial t} C_N$: the increase of C_N after the decrease of volume V_N.
- $-\frac{1}{\alpha}\frac{\partial \alpha}{\partial t} C_R$: the decrease of C_R after the increase of volume V_R.

Nevertheless, Eqs. (12) and (13) have one singularity each, α and $(1-\alpha)$, that may pose some problems in a rigorous numerical implementation. For this reason, later in the text, we will show that it is preferable to work with the variables C_1 and C_2.

We also compute the time derivative of the total concentration C_T to analyse its behaviour:

$$\frac{\partial C_T}{\partial t} = \frac{\partial}{\partial t}((1-\alpha)C_N) + \frac{\partial}{\partial t}(\alpha C_R) \tag{14}$$

Resulting in the sum of Eqs. (10) and (11):

$$\frac{\partial C_T}{\partial t} = -\frac{\partial \alpha}{\partial t} C_N + (1-\alpha)\frac{\partial C_N}{\partial t} + \frac{\partial \alpha}{\partial t} C_R + \alpha \frac{\partial C_R}{\partial t} \tag{15}$$

By substituting Eqs. (12) and (13) into the previous Eq. (15), it results that:

$$\frac{\partial C_T}{\partial t} = (1-\alpha) D_N \nabla^2 C_N + \alpha D_R \nabla^2 C_R + S \tag{16}$$

Eq. (16) states that the rate of change of the total concentration C_T over the control volume V is governed by two diffusional leakage terms (one per volume region), and the global production rate S. In particular:

- $\frac{\partial C_T}{\partial t}$ is referred to the total volume V.
- $(1-\alpha)D_N\nabla^2 C_N$ is referred to the volume V, thanks to the $(1-\alpha)$ term.
- Likewise, $\alpha D_R\nabla^2 C_R$ is referred to the volume V thanks to the α term.
- The source S is the production rate per unit volume.

2.2. Sweeping exchange term

In this Section, we apply a discrete approach to derive an exchange term of gas atoms from the non-restructured region N to the restructured one R. Given the control volume V, we suppose it is formed by a number n of volumes V_N and a number m of volumes V_R. Each volume V_N contains N_N atoms, and each V_R containing N_R atoms. We simplify the derivation by neglecting previously considered production and leakage terms.

Then, we assume a discrete increase of α during a single time step. Labelling with i the initial values:

$$C_{Ni} = \frac{nN_N}{nV_N} = \frac{N_N}{V_N} \tag{17}$$

and

$$C_{Ri} = \frac{mN_R}{mV_R} = \frac{N_R}{V_R} \tag{18}$$

We suppose that during the considered time step, a certain number k of volumes, together with the corresponding atoms, have transformed from V_N to V_R. Hence, labelling f the final values:

$$C_{Nf} = \frac{(n-k)N_N}{(n-k)V_N} = \frac{N_N}{V_N} \tag{19}$$

and

$$C_{Rf} = \frac{mN_R + kN_N}{mV_R + kV_N} \tag{20}$$

This discrete representation clearly shows how a pure restructuring operation does not influence C_N but only C_R. Eq. (20) can be worked out giving:

$$C_{Rf} = \frac{C_{Ri} + \frac{k}{m}\frac{N_N}{N_R}}{1 + \frac{k}{m}\frac{V_N}{V_R}} \tag{21}$$

In the reasonable hypothesis that during a single time step, the restructuring process transforms a limited portion of the control volume V, we can consider $k \ll n$ and $k \ll m$ and linearise the previous term to get $dC_R = C_f^R - C_i^R$ as:

$$dC_R = -C_{Ri}\frac{k}{m}\frac{V_N}{V_R} + \frac{k}{m}\frac{N_N}{V_R} - \frac{k^2}{m^2}\frac{N_N V_N}{(V_R)^2} \tag{22}$$

where again, the last term can be neglected, providing:

$$dC_R = -C_{Ri}\frac{k}{m}\frac{V_N}{V_R} + \frac{k}{m}\frac{N_N}{V_R} \tag{23}$$

By grouping $\frac{k}{m}\frac{V_N}{V_R}$, the following equation is obtained:

$$dC_R = \frac{k}{m}\frac{V_N}{V_R}(C_N - C_{Ri}) \tag{24}$$

If we introduce the discrete α terms.

$$\alpha_i = \frac{mV_R}{V}, \quad \alpha_f = \frac{mV_R + kV_N}{V} = \alpha_i + k\frac{V_N}{V} \tag{25}$$

we get:

$$\frac{\alpha_f - \alpha_i}{\alpha_i} = \frac{k}{m}\frac{V_N}{V_R} \tag{26}$$

Resulting in the following exchange term:

$$dC_R = \frac{d\alpha}{\alpha_i}(C_N - C_i^R) \tag{27}$$

Or, in the continuous limit:

$$\frac{\partial C_R}{\partial t} = \frac{1}{\alpha}\frac{\partial \alpha}{\partial t}(C_N - C_R) \tag{28}$$

Hence, Eq. (28) represents the pure sweeping term that transfers gas atoms from the non-restructured region N to restructured one R after a virtual step of the restructuring process. To express the exchange term (Eq. (28)) for C_1 and C_2, we must consider that during the restructuring process $dC_N = 0$ ($C_{Ni} = C_{Nf}$), while $dC_R \neq 0$. Namely:

$$\begin{cases} \frac{\partial C_N}{\partial t} = 0 \\ \frac{\partial C_R}{\partial t} = \frac{1}{\alpha}\frac{\partial \alpha}{\partial t}(C_N - C_R) \end{cases} \tag{29}$$

In terms of C_1 and C_2, we obtain:

$$\begin{cases} \frac{\partial \frac{C_1}{1-\alpha}}{\partial t} = 0 \\ \frac{\partial \frac{C_2}{\alpha}}{\partial t} = \frac{1}{\alpha}\frac{\partial \alpha}{\partial t}\left(\frac{C_1}{1-\alpha} - \frac{C_2}{\alpha}\right) \end{cases} \tag{30}$$

After expanding the product derivatives, the isolated exchange terms are:

$$\begin{cases} \frac{\partial C_1}{\partial t} = -\frac{1}{1-\alpha}\frac{\partial \alpha}{\partial t}C_1 \\ \frac{\partial C_2}{\partial t} = \frac{1}{1-\alpha}\frac{\partial \alpha}{\partial t}C_1 \end{cases} \tag{31}$$

Because of the linearity of the operations involved so far, we can use the superposition principle and incorporate Eq. (29) into Eqs. (12) and (13):

$$\frac{\partial C_N}{\partial t} = D_N\nabla^2 C_N + \frac{1}{1-\alpha}\frac{\partial \alpha}{\partial t}C_N + S \tag{32}$$

$$\frac{\partial C_R}{\partial t} = D_R\nabla^2 C_R - \frac{1}{\alpha}\frac{\partial \alpha}{\partial t}C_R + \frac{1}{\alpha}\frac{\partial \alpha}{\partial t}(C_N - C_R) + S \tag{33}$$

Or similarly, we can include Eq. (31) into Eqs. (8) and (9):

$$\begin{cases} \frac{\partial C_1}{\partial t} = D_N\nabla^2 C_1 - \frac{1}{1-\alpha}\frac{\partial \alpha}{\partial t}C_1 + (1-\alpha)S \\ \frac{\partial C_2}{\partial t} = D_R\nabla^2 C_2 + \frac{1}{1-\alpha}\frac{\partial \alpha}{\partial t}C_1 + \alpha S \end{cases} \tag{34}$$

The last system of equations gives a simple and consistent representation of the mass balances due to production, leakage, and gas sweeping from phase N to phase R in the volume V.

3. Application to fission gas depletion in HBS

In this Section, Eq. (34) is applied in the SCIANTIX code (Zullo et al., 2023; Pizzocri et al., 2020) to assess the prediction of the fission gas depletion process. In particular, with the SCIANTIX code, we consider the state-of-the-art representation of the fission gas diffusion problem (Rest et al., 2019; Barani et al., 2020; Booth, 1957; Pastore et al., 2013). Summarising, the working hypotheses are the following:

- The single fuel grain is modelled as a spherical domain.
- In line with the new SCIANTIX 2.0 code structure, we consider two phases of the UO_2. The non-restructured and restructured UO_2 (i.e., UO_2-HBS). Each phase features its properties, e.g., different grain sizes.
- Each UO_2 phase forms a dedicated system (e.g., Xe-in-UO_2 and Xe-in-UO_2-HBS), each one with its specific properties (e.g., the diffusivity of xenon in the fuel matrix).

With the conventional symmetry boundary conditions at the centre of the spherical domain and perfect sink boundary conditions at the border of the spherical domain (Booth, 1957; Speight, 1969; Forsberg and Massih, 1985a,b; Pastore et al., 2013; Pizzocri et al., 2016; Pastore et al., 2018; Zullo et al., 2022). On top of the fission gas behaviour operated by SCIANTIX (e.g., the evolution of the intra-granular bubble

Table 1
Values of the model parameters.

Matrix	Parameter	Value	Reference
UO_2	D	$D = D_1 + D_2 + D_3$	Turnbull et al. (1989)
UO_2	a_1, grain size	5 μm	Olander (1976)
UO_2	g, trapping rate	$g = 4\pi D N_{ig} R_{ig}$	Ham (1958)
UO_2	b, re-solution rate	$b = 2\pi\mu_{ff}\dot{F}(R_{ig} + R_{ff})^2$	Olander and Wongsawaeng (2006)
UO_2-HBS	D	$D = 4.5 \times 10^{-42}\dot{F}$	Pizzocri et al. (2017), Barani et al. (2020)
UO_2-HBS	a_2, grain size	150 nm	Ray et al. (1997), Barani et al. (2020)

population (Zullo et al., 2023; Pizzocri et al., 2020, 2018)), we consider the following fission gas diffusion problem:

$$\begin{cases} \dfrac{\partial C_1}{\partial t} = \dfrac{D_1}{a_1^2}\nabla^2 C_1 - gC_1 + bm_1 - \dfrac{1}{1-\alpha}\dfrac{\partial \alpha}{\partial t}C_1 + (1-\alpha)S \\ \dfrac{\partial m_1}{\partial t} = gC_1 - bm_1 - \dfrac{1}{1-\alpha}\dfrac{\partial \alpha}{\partial t}m_1 \\ \dfrac{\partial C_2}{\partial t} = \dfrac{D_2}{a_2^2}\nabla^2 C_2 + \dfrac{1}{1-\alpha}\dfrac{\partial \alpha}{\partial t}(C_1 + m_1) + \alpha S \end{cases} \tag{35}$$

With a_1 and a_2 the radius of the fuel grain in non-restructured UO_2 and in restructured UO_2, respectively. Numerical values are given in Table 1. Eq. (35) represent the extended intra-granular problem that we solve in SCIANTIX, tailored to represent a smooth transition from UO_2 to UO_2-HBS phase. In particular,

- C_1 represents the concentration of fission gas in dynamic solution within the non-restructured matrix.
- m_1 represents the concentration of fission gas trapped in intra-granular bubbles within the non-restructured matrix.
- C_2 represents the concentration of fission gas in dynamic solution within the restructured matrix.

Since the intra-granular diffusion problem we consider with SCIANTIX is discretised with a spectral diffusion algorithm, we avoid solving the first two differential equations on the non-restructured micron-sized fuel grain and the third one on the restructured nanometric fuel grain by non-dimensionalising the Laplace operator. In other words, we solve the diffusion problem on the unit-radius sphere without changing the system eigenvalues $\frac{\pi^2 D}{a^2}k^2$ (Zullo et al., 2022).

We consider the restructured volume fraction proposed by Barani and co-workers (Barani et al., 2020, 2022):

$$\alpha = 1 - \exp\left(-2.77 \times 10^{-7}\beta_{\text{eff}}^{3.54}\right) \tag{36}$$

The restructured volume fraction α is proportional to the local effective burnup β_{eff}, used as a virtual threshold to define the HBS formation at temperature lower than the healing temperature threshold (T_{th} = 1273.15 K):

$$\beta_{\text{eff}} = \int H(T_{\text{th}})\,\mathrm{d}\,\beta \tag{37}$$

where β (MWd kgU^{-1}) is the fuel local burnup, and H is the Heaviside function (Khvostov et al., 2005; Holt et al., 2014; Pizzocri et al., 2017).

4. Results and discussion

We applied the previous modelling approach to simulate the behaviour of a representative Light Water Reactor (LWR) fuel pellet rim portion with SCIANTIX. Namely, we considered a steady-state irradiation history up to 200 GWd/tU at low temperature (723 K) and high fission rate (2×10^{19} fiss m^{-3} s^{-1}). Figs. 1 and 2 show the results obtained from solving Eq. (35). To evaluate the impact of the sweeping term (Eq. (31)), Fig. 1 is obtained by neglecting such term while it is considered in Fig. 2.

Moreover, Figs. 1 and 2 include separate contributions for xenon concentrations retained in UO_2 matrix:

- The contribution from the xenon retained in non-restructured UO_2 grains ($C_1 + m_1$).

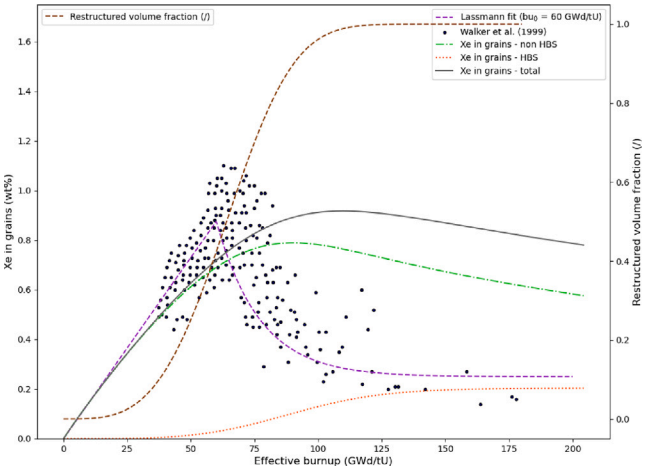

Fig. 1. Intra-granular xenon concentration calculated with the present model, without the sweeping term, as a function of local effective burnup. The comparison with the model from Lassmann et al. (1995b), is reported (purple dotted line), together with experimental data measured by EPMA on several samples (black dots, from Walker, 1999).

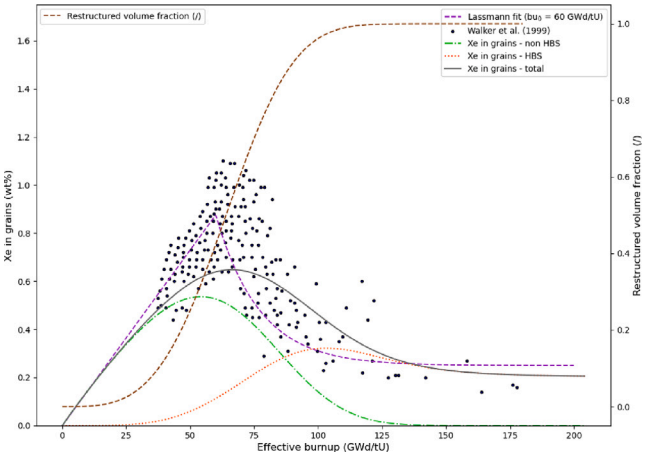

Fig. 2. Intra-granular xenon concentration calculated with the present model, including the sweeping term, as a function of local effective burnup. The comparison with the model from Lassmann et al. (1995b), is reported (purple dotted line), together with experimental data measured by EPMA on several samples (black dots, from Walker, 1999).

- The contribution from the xenon retained in restructured UO_2 grains (C_2)

and their sum. We stress again that the only purpose of Fig. 1 is to clarify the impact of the sweeping term which ensures a more realistic representation of the xenon depletion process together with advantages of numerical and implementation-wise nature. In particular, moving from Figs. 1 to 2, it can be noted that the mass transfer between the two matrix phases is responsible for the smooth decrease of the retained gas in reasonable agreement with available measured

data (from Walker, 1999). Moreover, the tail of the calculated intra-granular xenon concentration depends on the grain size of the UO_2-HBS matrix (i.e., asymptotic gas concentration). We use a value of 150 nm (Table 1), that is in line with experimental observations (Cappia et al., 2016, 2022; McKinney et al., 2023; Noirot et al., 2008; Khvostov et al., 2005) and previous modelling approaches (Lassmann et al., 1995a; Veshchunov and Shestak, 2009; Veshchunov et al., 2006; Pizzocri et al., 2017; Barani et al., 2020), and that agrees with the experimental data considered in Fig. 2. On the other hand, such grain size has its degree of intrinsic uncertainty (Pizzocri et al., 2017; Barani et al., 2020). The experimental data in Fig. 2 comes from different irradiation conditions and initial fuel characteristics. Considering the scattering of the considered data, the agreement can be regarded as acceptable (Lassmann et al., 1995b). Some degree of uncertainty must be necessarily taken into consideration, for instance, in the single-atom diffusivities of the xenon in the fuel matrices (reported in Table 1), regarding the experimental characterisation, which in principle could allow us to consider different (but reasonable) initial fuel grain sizes. Most importantly, some uncertainty must be ascribed to the 0-dimensional simulation we are performing with the SCIANTIX code, considering that a constant temperature and constant fission rate are not fully representative of the local temperature and burnup gradients. For instance, uncertainty is brought to the predicted position of the peak of the retained xenon ($\sim$ 60 GWd/tU in the considered simulation), which depends on the restructured volume fraction α, and on the local burnup itself. Further refinement of this feature is to be considered in a more detailed representation of the restructured volume fraction, possibly including other quantities like the dislocation density as it was done in other works (Veshchunov et al., 2006; Veshchunov and Shestak, 2009). Issues of this kind have been addressed and detailed in previous works (Pizzocri et al., 2017; Barani et al., 2020), and a similar examination and comparison are valid for the present work.

5. Conclusions

This work outlines a modelling approach to describe the intra-granular fission gas behaviour in UO_2, considering the evolution of the non-restructured and restructured fuel matrices. The model leverages the definition of the restructured volume fraction, which currently depends on the local effective burnup. The primary outcome of the model is a simple yet effective description of two intra-granular gas diffusion problems interconnected by an exchange term, sweeping gas atoms from one phase to the other. In addition, by leveraging the spectral diffusion algorithm for the intra-granular fission gas problem, we avoided dealing with two different integration domains (micrometric and sub-micrometric grains) and solved a single spatial dimensionless problem. The model developed has been implemented in SCIANTIX, a 0D meso-scale code for physics-based modelling of fission gases in nuclear oxide fuel and compared with experimental data and semi-empirical models. The model results are consistent with the experimental data and past semi-empirical models, with the sweeping term providing a smooth representation of the xenon depletion in forming HBS.

CRediT authorship contribution statement

G. Zullo: Writing – original draft, Visualization, Software, Methodology, Investigation, Data curation, Conceptualization. **A. Scolaro:** Writing – review & editing, Supervision, Conceptualization. **T. Barani:** Writing – review & editing, Supervision, Conceptualization. **D. Pizzocri:** Writing – review & editing, Supervision, Project administration, Methodology.

Declaration of competing interest

The authors declare that they have no known competing financial interests or personal relationships that could have appeared to influence the work reported in this paper.

Data availability

Data will be made available on request.

Acknowledgements

This work has been partially supported by the ENEN2plus project (HORIZON-EURATOM-2021-NRT-01-13 101061677) founded by the European Union. This project has received funding from the Euratom Research and Training Programme 2021–2027 through the OperaHPC project under grant agreement n^o 101061453.

References

Barani, T., Pizzocri, D., Cappia, F., Luzzi, L., Pastore, G., Van Uffelen, P., 2020. Modeling high burnup structure in oxide fuels for application to fuel performance codes. Part I: High burnup structure formation. J. Nucl. Mater. 539, 152296. http://dx.doi.org/10.1016/J.JNUCMAT.2020.152296.

Barani, T., Pizzocri, D., Cappia, F., Pastore, G., Luzzi, L., Van Uffelen, P., 2022. Modeling high burnup structure in oxide fuels for application to fuel performance codes. Part II: Porosity evolution. J. Nucl. Mater. 563, 153627. http://dx.doi.org/10.1016/J.JNUCMAT.2022.153627.

Booth, A., 1957. A method of calculating fission gas diffusion from UO_2 fuel and its application to the X-2-f loop test. URL https://www.osti.gov/biblio/4331839.

Burke, J.E., Turnbull, D., 1952. Recrystallization and grain growth. Prog. Metal Phys. 3, 220–292. http://dx.doi.org/10.1016/0502-8205(52)90009-9.

Cappia, F., Pizzocri, D., Schubert, A., Uffelen, P.V., Paperini, G., Pellottiero, D., Macián-Juan, R., Rondinella, V.V., 2016. Critical assessment of the pore size distribution in the rim region of high burnup UO2 fuels. J. Nucl. Mater. 480, 138–149. http://dx.doi.org/10.1016/J.JNUCMAT.2016.08.010.

Cappia, F., Wright, K., Frazer, D., Bawane, K., Kombaiah, B., Williams, W., Finkeldei, S., Teng, F., Giglio, J., Cinbiz, M.N., Hilton, B., Strumpell, J., Daum, R., Yueh, K., Jensen, C., Wachs, D., 2022. Detailed characterization of a PWR fuel rod at high burnup in support of LOCA testing. J. Nucl. Mater. 569, 153881. http://dx.doi.org/10.1016/J.JNUCMAT.2022.153881.

Cunningham, M.E., Freshley, M.D., Lanning, D.D., 1992. Development and characteristics of the rim region in high burnup UO_2 fuel pellets. J. Nucl. Mater. 188, 19–27. http://dx.doi.org/10.1016/0022-3115(92)90449-U.

Forsberg, K., Massih, A.R., 1985a. Diffusion theory of fission gas migration in irradiated nuclear fuel UO_2. J. Nucl. Mater. 135, http://dx.doi.org/10.1016/0022-3115(85)90071-6.

Forsberg, K., Massih, A.R., 1985b. Fission gas release under time-varying conditions. J. Nucl. Mater. 127, http://dx.doi.org/10.1016/0022-3115(85)90348-4.

Gerczak, T.J., Parish, C.M., Edmondson, P.D., Baldwin, C.A., Terrani, K.A., 2018. Restructuring in high burnup UO2 studied using modern electron microscopy. J. Nucl. Mater. 509, 245–259. http://dx.doi.org/10.1016/J.JNUCMAT.2018.05.077.

Ham, F.S., 1958. Theory of diffusion-limited precipitation. J. Phys. Chem. Solids 6, 335–351. http://dx.doi.org/10.1016/0022-3697(58)90053-2.

Holt, L., Schubert, A., Uffelen, P.V., Walker, C.T., Fridman, E., Sonoda, T., 2014. Sensitivity study on xe depletion in the high burn-up structure of UO 2. J. Nucl. Mater. 452, 166–172. http://dx.doi.org/10.1016/j.jnucmat.2014.05.009.

Jernkvist, L., 2019. Modelling of fine fragmentation and fission gas release of UO_2 fuel in accident conditions. EPJ Nucl. Sci. Technol. 5, 11. http://dx.doi.org/10.1051/EPJN/2019030, https://www.epj-n.org/articles/epjn/full_html/2019/01/epjn190024/epjn190024.htmlhttps://www.epj-n.org/articles/epjn/abs/2019/01/epjn190024/epjn190024.html.

Jernkvist, L., 2020. A review of analytical criteria for fission gas induced fragmentation of oxide fuel in accident conditions. Prog. Nucl. Energy 119, 103188. http://dx.doi.org/10.1016/j.pnucene.2019.103188.

Khvostov, G., Novikov, V., Medvedev, A., Bogatyr, S., 2005. Approaches to Modeling of High Burn-up Structure and Analysis of its Effects on the Behaviour of Light Water Reactor Fuels in the START-3 Fuel Performance Code. In: Conference: 2005 Water Reactor Fuel Performance Meeting. Kyoto, Japan.

Lassmann, K., Walker, C.T., van de Laar, J., Lindström, F., 1995a. Modelling the high burnup UO_2 structure in LWR fuel. J. Nucl. Mater. 226, 1–8. http://dx.doi.org/10.1016/0022-3115(95)00116-6.

Lassmann, K., Walker, C.T., van de Laar, J., Lindström, F., 1995b. Modelling the high burnup UO_2 structure in LWR fuel. J. Nucl. Mater. 226, 1–8. http://dx.doi.org/10.1016/0022-3115(95)00116-6.

Lemes, M., Soba, A., Denis, A., 2014. An empirical formulation to describe the evolution of the high burnup structure. http://dx.doi.org/10.1016/j.jnucmat.2014.09.048, URL http://dx.doi.org/10.1016/j.jnucmat.2014.09.048.

McKinney, C., Seibert, R., Werden, J., Parish, C., Gerczak, T., Harp, J., Capps, N., 2023. Characterization of the radial microstructural evolution in LWR UO2 using electron backscatter diffraction. J. Nucl. Mater. 585, 154605. http://dx.doi.org/10.1016/J.JNUCMAT.2023.154605.

Noirot, J., Desgranges, L., Lamontagne, J., 2008. Detailed characterisations of high burn-up structures in oxide fuels. J. Nucl. Mater. 372, 318–339. http://dx.doi.org/10.1016/j.jnucmat.2007.04.037.

Olander, D., 1976. Fundamental Aspects of Nuclear Reactor Fuel Elements. Technical lnformation Center Energy Research and Development Administration.

Olander, D.R., Wongsawaeng, D., 2006. Re-solution of fission gas - A review: Part I. Intragranular bubbles. J. Nucl. Mater. 354, 94–109. http://dx.doi.org/10.1016/j.jnucmat.2006.03.010.

Pastore, G., Luzzi, L., Di Marcello, V., Uffelen, P.V., 2013. Physics-based modelling of fission gas swelling and release in UO_2 applied to integral fuel rod analysis. Nucl. Eng. Des. 256, 75–86. http://dx.doi.org/10.1016/j.nucengdes.2012.12.002.

Pastore, G., Pizzocri, D., Rabiti, C., Barani, T., Uffelen, P.V., Luzzi, L., 2018. An effective numerical algorithm for intra-granular fission gas release during non-equilibrium trapping and resolution. J. Nucl. Mater. 509, 687–699. http://dx.doi.org/10.1016/j.jnucmat.2018.07.030.

Pizzocri, D., Barani, T., Luzzi, L., 2020. SCIANTIX: A new open source multi-scale code for fission gas behaviour modelling designed for nuclear fuel performance codes. J. Nucl. Mater. 532, 152042. http://dx.doi.org/10.1016/j.jnucmat.2020.152042.

Pizzocri, D., Cappia, F., Luzzi, L., Pastore, G., Rondinella, V.V., Van Uffelen, P., 2017. A semi-empirical model for the formation and depletion of the high burnup structure in UO2. J. Nucl. Mater. 487, 23–29. http://dx.doi.org/10.1016/j.jnucmat.2017.01.053.

Pizzocri, D., Pastore, G., Barani, T., Magni, A., Luzzi, L., Uffelen, P.V., Pitts, S.A., Alfonsi, A., Hales, J.D., 2018. A model describing intra-granular fission gas behaviour in oxide fuel for advanced engineering tools. J. Nucl. Mater. 502, 323–330. http://dx.doi.org/10.1016/j.jnucmat.2018.02.024.

Pizzocri, D., Rabiti, C., Luzzi, L., Barani, T., Van Uffelen, P., Pastore, G., 2016. PolyPole-1: An accurate numerical algorithm for intra-granular fission gas release. J. Nucl. Mater. 478, 333–342. http://dx.doi.org/10.1016/j.jnucmat.2016.06.028.

Ray, I.L.F., Matzke, H.J., Thiele, H.A., Kinoshita, M., 1997. An electron microscopy study of the RIM structure of a UO_2 fuel with a high burnup of 7.9% FIMA. J. Nucl. Mater. 245, 115–123. http://dx.doi.org/10.1016/S0022-3115(97)00015-9.

Rest, J., Cooper, M.W., Spino, J., Turnbull, J.A., Van Uffelen, P., Walker, C.T., 2019. Fission gas release from UO2 nuclear fuel: A review. J. Nucl. Mater. 513, 310–345. http://dx.doi.org/10.1016/j.jnucmat.2018.08.019.

Speight, M., 1969. A calculation on the migration of fission gas in material exhibiting precipitation and re-solution of gas atoms under irradiation. Nucl. Sci. Eng. 37, 180–185. http://dx.doi.org/10.13182/nse69-a20676.

Spino, J., Rest, J., Goll, W., Walker, C.T., 2005. Matrix swelling rate and cavity volume balance of UO2 fuels at high burn-up. J. Nucl. Mater. 346, 131–144. http://dx.doi.org/10.1016/j.jnucmat.2005.06.015.

Spino, J., Stalios, A.D., Cruz, H.S., Baron, D., 2006. Stereological evolution of the rim structure in PWR-fuels at prolonged irradiation: Dependencies with burn-up and temperature. J. Nucl. Mater. 354, 66–84. http://dx.doi.org/10.1016/J.JNUCMAT.2006.02.095.

Turnbull, J.A., White, R.J., Wise, C., 1989. The diffusion coefficient for fission gas atoms in uranium dioxide. URL https://inis.iaea.org/search/search.aspx?orig_q=RN:21003206.

Veshchunov, M.S., Ozrin, V.D., Shestak, V.E., Tarasov, V.I., Dubourg, R., Nicaise, G., 2006. Development of the mechanistic code MFPR for modelling fission-product release from irradiated UO_2 fuel. Nucl. Eng. Des. 236, 179–200. http://dx.doi.org/10.1016/j.nucengdes.2005.08.006.

Veshchunov, M.S., Shestak, V.E., 2009. Model for evolution of crystal defects in UO_2 under irradiation up to high burn-ups. J. Nucl. Mater. 384, 12–18. http://dx.doi.org/10.1016/J.JNUCMAT.2008.09.024.

Walker, C., 1999. Assessment of the radial extent and completion of recrystallisation in high burn-up UO_2 nuclear fuel by EPMA. J. Nucl. Mater. 275, 56–62. http://dx.doi.org/10.1016/S0022-3115(99)00108-7.

Walker, C.T., Kameyama, T., Kitajima, S., Kinoshita, M., 1992. Concerning the microstructure changes that occur at the surface of UO2 pellets on irradiation to high burnup. J. Nucl. Mater. 188, 73–79. http://dx.doi.org/10.1016/0022-3115(92)90456-U.

Wiss, T., Rondinella, V.V., Konings, R.J., Staicu, D., Papaioannou, D., Bremier, S., Pöml, P., Benes, O., Colle, J.Y., Uffelen, P.V., Schubert, A., Cappia, F., Marchetti, M., Pizzocri, D., Jatuff, F., Goll, W., Sonoda, T., Sasahara, A., Kitajima, S., Kinoshita, M., 2017. Properties of the high burnup structure in nuclear light water reactor fuel. Radiochim. Acta 105, 893–906. http://dx.doi.org/10.1515/ract-2017-2831.

Zullo, G., Pizzocri, D., Luzzi, L., 2022. On the use of spectral algorithms for the prediction of short-lived volatile fission product release: Methodology for bounding numerical error. Nucl. Eng. Technol. 54, 1195–1205. http://dx.doi.org/10.1016/J.NET.2021.10.028.

Zullo, G., Pizzocri, D., Luzzi, L., 2023. The SCIANTIX code for fission gas behaviour: Status, upgrades, separate-effect validation, and future developments. J. Nucl. Mater. 587, 154744. http://dx.doi.org/10.1016/J.JNUCMAT.2023.154744.